A Simple Model for Predicting Tropical Cyclone Minimum Central Pressure from Intensity and Size

DANIEL R. CHAVAS,[a] JOHN A. KNAFF,[b] AND PHIL KLOTZBACH[c]

[a] *Department of Earth, Atmospheric, and Planetary Sciences, Purdue University, West Lafayette, Indiana*
[b] *NOAA/Center for Satellite Applications and Research, Fort Collins, Colorado*
[c] *Department of Atmospheric Science, Colorado State University, Fort Collins, Colorado*

(Manuscript received 21 February 2024, in final form 22 July 2024, accepted 15 August 2024)

ABSTRACT: Minimum central pressure (P_{min}) is an integrated measure of the tropical cyclone wind field and is known to be a useful indicator of storm damage potential. A simple model that predicts P_{min} from routinely estimated quantities, including storm size, would be of great value. Here, we present a simple linear empirical model for predicting P_{min} from maximum wind speed, a radius of 34-kt (1 kt $\approx$ 0.51 m s^{-1}) winds (R_{34kt}), storm center latitude, and the environmental pressure. An empirical model for the pressure deficit is first developed that takes as predictors specific combinations of these quantities that are derived directly from theory based on gradient wind balance and a modified Rankine-type wind profile known to capture storm structure inside of R_{34kt}. Model coefficients are estimated using data from the southwestern North Atlantic and eastern North Pacific from 2004 to 2022 using aircraft-based estimates of P_{min}, extended best track data, and estimates of environmental pressure from Global Forecast System (GFS) analyses. The model has a near-zero conditional bias even for low P_{min}, explaining 94.2% of the variance. Performance is superior to a variety of other model formulations, including a standard wind–pressure model that does not account for storm size or latitude (89.2% variance explained). Model performance is also strong when applied to high-latitude data and data near coastlines. Finally, the model is shown to perform comparably well in an operation-like setting based solely on routinely estimated variables, including the pressure of the outermost closed isobar. Case study applications to five impactful historical storms are discussed. Overall, the model offers a simple, fast, physically based prediction for P_{min} for practical use in operations and research.

SIGNIFICANCE STATEMENT: Sea level pressure is lowest at the center of a hurricane and is routinely estimated in operational forecasting along with the maximum wind speed. While the latter is currently used to define hurricane intensity, the minimum pressure is also a viable measure of storm intensity that is known to better represent damage risk. A simple empirical model that predicts the minimum pressure from maximum wind speed and size, and based on the physics of the hurricane wind field, does not currently exist. This work develops such a model by using wind field physics to determine the important parameters and then uses a simple statistical model to make the final prediction. This model is quick and easy to use in weather forecasting and risk assessment applications.

KEYWORDS: Tropical cyclones; Hurricanes/typhoons; Operational forecasting; Risk assessment

1. Introduction

At 2100 UTC 22 September 2005, the National Hurricane Center forecast discussion for Hurricane Rita stated "The minimum central pressure has remained around 913 mb … which is a very low pressure to have only 125 knots." This statement reflects a relatively infrequent but important issue when the minimum central pressure in a tropical cyclone differs strongly from what would be "expected" from its maximum wind speed alone based on historical experience. This example emphasizes the confusion that arises when our two common measures of tropical cyclone intensity—the point maximum wind speed V_{max}, which is the official measure of the Saffir–Simpson hurricane wind scale, and the minimum central pressure P_{min}—depart from one another. This confusion begins with the attempt to characterize a storm's strength scientifically but then extends to the translation of this characterization into potential implications for the general public.

Indeed, it has long been standard to convert between the tropical cyclone maximum wind speed and P_{min} using a simple empirical wind–pressure relation (Dvorak 1975, 1984; Atkinson and Holliday 1977; Koba et al. 1990; Knaff and Zehr 2007, hereafter KZ07; Courtney and Knaff 2009). This one-to-one relation assumes that P_{min} depends predominantly on V_{max}. KZ07 demonstrated that minimum pressure also depends secondarily on storm size and latitude, motivated by gradient wind balance. This latter result was explained physically by Chavas et al. (2017) by combining gradient wind balance with a theoretical wind structure model. Chavas et al. (2017) demonstrated that a simple linear model that depends on V_{max} and the product of

Denotes content that is immediately available upon publication as open access.

Supplemental information related to this paper is available at the Journals Online website: https://doi.org/10.1175/WAF-D-24-0031.s1.

Corresponding author: Daniel R. Chavas, drchavas@gmail.com

DOI: 10.1175/WAF-D-24-0031.1

outer size and the Coriolis parameter successfully predicted the central pressure deficit in simulations and observations. However, that work employed as its size metric a radius of 8 m s^{-1}, which is not routinely estimated operationally nor reanalyzed for retention in a long-term archive. As a result, the utility of this model has been limited. A predictive[1] model aligned with Chavas et al. (2017) that takes as input parameters that are routinely estimated in operations would be much more useful.

The potential utility of a precise and easy-to-use model for P_{min} has grown as recent work has directly connected P_{min} to risk. The variable P_{min} is a remarkably good predictor of the normalized economic damage that has been wrought by landfalling hurricanes in the continental United States (Bakkensen and Mendelsohn 2016; Klotzbach et al. 2020, 2022). Klotzbach et al. (2020) demonstrated that P_{min} is a substantially better predictor than V_{max}, particularly for hurricanes making landfall from Georgia to Maine where weaker but larger storms are more common. Klotzbach et al. (2022) demonstrated that P_{min} is also at least as good of a predictor as integrated measures of the near-surface wind field, including both integrated kinetic energy and integrated power dissipation, that inherently require data from the entire wind field to estimate. The explanation lies in the fact that P_{min} is itself an integrated measure of the wind field that accounts for both maximum wind speed and storm size (Chavas et al. 2017). The total wind field drives the wind, storm surge, and rainfall hazards that ultimately cause damage and loss of life (Irish and Resio 2010; Zhai and Jiang 2014). Hence, P_{min} appears to be an especially well-suited measure of the damage potential of a storm, and it carries ancillary practical benefits.

First, P_{min} is relatively easy to estimate, as it requires a relatively few observations within a small area near the storm center and, moreover, it varies relatively smoothly in space and time since it is by definition an integrated quantity (either in radius via gradient wind balance or in height via hydrostatic balance). In contrast, V_{max} is a local estimate at a single point of a quantity that is inherently noisy and hence is notoriously difficult to estimate from sparse observations (Uhlhorn and Nolan 2012). Second, P_{min} is already routinely estimated operationally; indeed, it was used in conjunction with the maximum wind speed as part of the Saffir–Simpson Scale prior to 2009 (Schott et al. 2012).

The practical benefits of a model for P_{min} extend beyond operations to climate and risk modeling. Climate models are better able to reproduce the historical distribution of minimum pressure than maximum wind speed (Knutson et al. 2015), suggesting that the former is a more stable and suitable metric for model evaluation and intercomparison (Zarzycki et al. 2021). For risk modeling, the pressure field is included as input in storm surge models (Gori et al. 2023). More generally, a model that can relate P_{min}, V_{max}, and size to one another should enable the use of all available data to more precisely constrain the properties of historical tropical cyclones and their relationships to hazards and potential impacts.

Here, our objective is to create a simple model to predict P_{min} that can be easily used in operations and practical applications. The spirit of this effort to make theory directly useful for the community follows from a similar effort for predicting R_{max} presented in Chavas and Knaff (2022) and Avenas et al. (2023). Section 2 describes the datasets used in our analysis. Section 3 develops the empirical model and its physical basis. Section 4 estimates model parameters from data and applies the model in a few notable contexts, including an operational setting using only routinely estimated parameters. Section 5 provides a brief summary and discussion.

2. Data and methods

Our dataset combines flight-based data for P_{min}, final best track data for storm central latitude, maximum wind speed V_{max}, a quadrant-maximum radius of 34-kt wind (R_{34kt}; 1 kt ≈ 0.51 m s^{-1}), storm translation speed V_{trans}, and estimates of environmental pressure P_{env} from analysis and best track data. We use R_{34kt} because it is the outermost radius routinely estimated operationally. We analyze storms in both the North Atlantic and eastern North Pacific basins for the period 2004–22, where 2004 is the first year in which postseason best tracking of R_{34kt} was performed. All information is contained in the databases of the Automated Tropical Cyclone Forecast (ATCF) system (Sampson and Schrader 2000). These data are identical to that available in the extended best track (EBTRK, Demuth et al. 2006).

Direct observational estimates of P_{min} are critical to ensure that these data are true independent observations and are not inferred from V_{max} via an existing wind–pressure relationship (which is difficult to determine in retrospect), as this would undercut the purpose of our work. Hence, we take P_{min} estimates based on aircraft and recorded in the ATCF databases. We then linearly interpolate best track data to the times of flight-based estimates of P_{min}. Following DeMaria et al. (2009) and Chavas and Knaff (2022), we calculate the mean radius of 34-kt wind at a given time, hereafter $\overline{R}_{34kt}$, by averaging all nonzero quadrant values and then multiplying the result by 0.85 to account for the fact that the quadrant values are defined as the maximum extent in that quadrant and are not the mean:

$$\overline{R}_{34kt} = 0.85\left(\frac{1}{n}\sum_{i=1}^{n} R^{i}_{34kt}\right), \tag{1}$$

where n is the number of nonzero quadrant values. Finally, to estimate the azimuthal-mean maximum wind speed $\overline{V}_{max}$, we follow the simple method of Lin and Chavas (2012) and subtract 55% of the translation speed from the best track V_{max}:

$$\overline{V}_{max} = V_{max} - 0.55V_{trans}. \tag{2}$$

The variable V_{trans} is calculated from the mean displacement between the TC location at the given time and 12 h prior (so as to be operationally predictive), with best track latitude and

[1] Note: we use "predictive" here in the statistical sense (modeling one parameter from other concurrent parameters) rather than the forecasting sense (modeling the future).

longitude, each linearly interpolated to the relevant times. In our results below, we test the effect of including this translation modification and also compare with the nonlinear translation speed reduction of KZ07.

A combination of the NCEP Climate Forecast System (CFS; Saha et al. 2014) and Global Forecast System (GFS) analyses (GFS 2021) were used to estimate P_{env}. CFS analyses were used in 2004 and 2005, and GFS analyses were used thereafter. We use the profile of tangential wind in the analysis, specifically a radius of 8 m s^{-1} (R_{8ms}), to inform us what radius represents the outer edge of the storm and to calculate P_{env}. The variable P_{env} was calculated at 900 km for R_{8ms} = 0–600 km, 1200 km for R_{8ms} = 600–900 km, 1500 km for R_{8ms} = 900–1200 km, 1800 km for R_{8ms} = 900–1200 km, and 2100 km for R_{8ms} = 1200–1500 km. In the final section, we also estimate the environmental pressure for operational relevance using the pressure of the outermost closed isobar (P_{oci}) extracted from the ATCF databases or EBTRK dataset.

Following Chavas and Knaff (2022), to develop our model, we filter our data to focus on a subset of high-quality cases over the open ocean within the tropical western Atlantic basin where aircraft reconnaissance is routine. Hence, we restrict our data to cases west of 50°W and south of 30°N and with $\overline{R}_{34kt}$ smaller than the distance from the storm center to the coastline. We only include cases with at least three nonzero quadrant values of R_{34kt} to ensure a reasonable estimate of the azimuthal-mean value, and where $\overline{V}_{max}$ is at least 20 m s^{-1} to avoid weak tropical storms and tropical depressions. A map of the final training dataset is displayed in Fig. 1a. As described below, we will also apply our model to additional subsets of data to explore its broader utility.

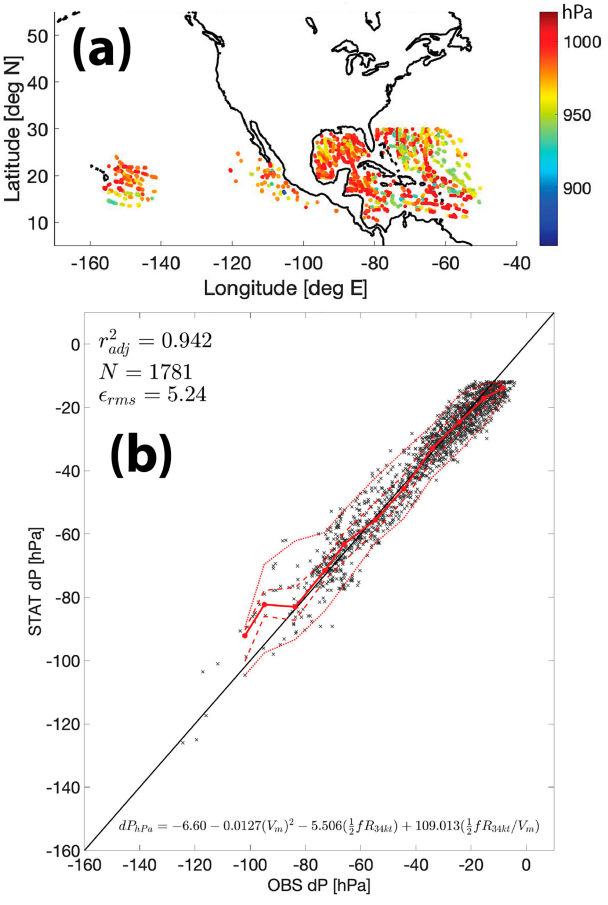

FIG. 1. (a) Map of the aircraft-based historical P_{min} dataset used in this study; the color denotes the magnitude of P_{min} (hPa). (b) Model prediction for ΔP [Eq. (5); y axis] vs observed ΔP (x axis) for all data shown in (a), with conditional median (red solid), interquartile range (red dashed), and 5%–95% range (red dotted).

3. Model for pressure deficit ΔP

The minimum pressure is given by

$$P_{min} = P_{env} + \Delta P, \tag{3}$$

where P_{min} is the minimum central pressure, P_{env} is the environmental pressure, and ΔP is the pressure deficit at the storm center (defined as negative for low pressure). Here, we develop a model specifically for ΔP, as this is what is tied physically to the wind field. We also test P_{min} alone below and demonstrate that the knowledge of P_{env} does add additional value. The practical use of the model is tackled in section 4c, where we combine our model prediction for ΔP with an estimate for P_{env} to predict P_{min} itself.

We develop a model for ΔP that is derived from gradient wind balance applied to a two-region, modified Rankine vortex model of the axisymmetric tropical cyclone wind field. The full derivation is presented in the appendix. Here, we focus on the core outcome from the theory. The term ΔP_{hPa} (hPa) depends linearly on three physical predictors: $\overline{V}^2_{max}$, $(1/2)f\overline{R}_{34kt}$, and $(1/2)f\overline{R}_{34kt}/\overline{V}_{max}$. The variable $\overline{V}_{max}$ is the azimuthal-mean maximum wind speed in units of meters per second; $\overline{R}_{34kt}$ is the radius of 34-kt winds in units meters (1 n mi = 1852 m); and f is the Coriolis parameter at the storm-center latitude (ϕ) in units of per second [$f = 2\Omega\sin(\phi)$, $\Omega = 7.292 \times 10^{-5}$ s^{-1}].

Because the theory has various approximations built into it, we do not use the final theoretical result [Eq. (A11)] directly but rather use theory simply to identify the predictors. We then model ΔP using a simple multiple linear regression (MLR) model using those predictors:

$$\Delta P_{hPa} = \beta_0 + \beta_{Vmax^2}(\overline{V}^2_{max}) + \beta_{fR}\left(\frac{1}{2}f\overline{R}_{34kt}\right) + \beta_{fRdV}\left(\frac{\frac{1}{2}f\overline{R}_{34kt}}{\overline{V}_{max}}\right). \tag{4}$$

This approach produces an optimal model that exploits the benefits of both theory and observational data. A similar approach was taken to predict the radius of maximum wind in Chavas and Knaff (2022) and Avenas et al. (2023). The first predictor ($\overline{V}^2_{max}$) captures the maximum wind speed dependence of the pressure drop; it arises from the cyclostrophic

component of gradient wind balance. The second predictor $[(1/2)f\overline{R}_{34kt}]$ captures the combined size and Coriolis dependence of the pressure drop; it arises from the size-dependent Coriolis component of gradient wind balance. The final predictor $[(1/2)fR_{34kt}/\overline{V}_{max}]$ enhances the pressure drop from $\overline{V}^2_{max}$ (its term is less positive at larger $\overline{V}_{max}$), and it opposes the pressure drop from $(1/2)fR_{34kt}$ (its term is more positive at larger R_{34kt} or f); its interpretation is more complex but is associated with the contraction of R_{max} as $\overline{V}_{max}$ increases. For a more detailed physical interpretation, see the appendix.

Briefly, we note the contrast with Chavas et al. (2017), which found a simpler multiple linear regression relationship for ΔP on $\overline{V}_{max}$ and $(1/2)fR$, where R was taken as the radius of 8 m s^{-1}. These two parameters were taken directly from the wind structure theory of Chavas and Lin (2016) applied to gradient wind balance, and indeed, they show up here too. However, since the theory of Chavas and Lin (2016) has no analytic solution, Chavas et al. (2017) could not derive an analytic solution for P_{min} and hence could not define exactly how P_{min} should depend on those parameters [their Eq. (12)]. Instead, they merely found that a pure linear dependence worked well. The new model presented here [Eq. (4)] now gives that analytic dependence. This dependence corroborates the results of Chavas et al. (2017) as both parameters appear in our first two terms, too, but with a slight deviation associated with the third term in Eq. (4) that depends on the ratio of the two parameters. Note that while it might seem desirable to take the reciprocal of the third term, this will make the dependence on the term nonlinear, and indeed doing so results in a significantly degraded performance.

To estimate model coefficients [Eq. (4)], we first bin the dataset into increments of 10 m s^{-1} for $\overline{V}_{max}$, 50 km for $\overline{R}_{34kt}$, and 10^{-5} s^{-1} for f (i.e., approximately 4° latitude) and calculate the median value of each of the three quantities within the bin, resulting in a single data point per joint $(\overline{V}_{max}, \overline{R}_{34kt}, f)$ bin. Binning minimizes the effects of variations in sample size across the phase space of these variables when estimating model parameters, and it also helps reduce noise within a given bin. No minimum sample size is imposed within each bin, so all bins with at least one valid data point are retained to ensure more extreme cases are included in the fitting. Multiple linear regression coefficients are calculated using the fitlm function in MATLAB. We use the entire dataset in order to produce the best estimate of the model coefficients from all available data. We estimate the 95% confidence interval of each model coefficient as the 2.5th and 97.5th percentiles from a 1000-member bootstrap with resampling of the raw dataset, each fit following the same procedure as above. We explicitly account for the number of degrees of freedom in model performance metrics by calculating the adjusted r-squared value reduced from the nominal value based on the number of degrees of freedom relative to the sample size, $r^2_{adj} = 1 - [(n-1)/(n-p)](SSE/SST)$, where n is the sample size, p is the number of coefficients, SSE is the sum of squared error, and SST is the sum of squared total. The adjustment factor $(n-1)/(n-p)$ is very small (≈1.0017, i.e., a 0.17% reduction from nominal) since the number of coefficients $p = 4$ is much smaller than our sample size of approximately 1700, indicating that model overfitting is not a concern. This approach is analogous to removing an arbitrary subset of years for out-of-sample validation, and it carries the added benefit of allowing us to use the entire dataset to yield the best possible coefficient estimates. Nonetheless, we also test our model against multiple out-of-sample subsets described below that further demonstrate the generality of the model. To evaluate model performance, we apply the model described above to the full, raw dataset and quantify the statistics of the observed versus predicted ΔP or P_{min}.

We first present the final model and its performance. We then demonstrate the utility of each term in the model, including a comparison with a standard "wind–pressure" model in which $\overline{V}_{max}$ is the only predictor. We then apply the model to a few specific out-of-sample applications that are of practical interest. Finally, we show how to use the model in an operational setting using only routinely estimated data and examine model performance for a few case studies of impactful storms in the recent historical record.

4. Results

a. Model results

Our final model is

$$\Delta P_{hPa} = -6.60 - 0.0127(\overline{V}^2_{max}) - 5.506\left(\frac{1}{2}f\overline{R}_{34kt}\right) + 109.013\left(\frac{\frac{1}{2}f\overline{R}_{34kt}}{\overline{V}_{max}}\right), \quad (5)$$

with ΔP_{hPa} in units of hectopascals, $\overline{V}_{max}$ in units of meters per second, $\overline{R}_{34kt}$ in units of meters, and f in units of per second. As described in section 2, the coefficient values are estimated by fitting the model to the dataset binned in fixed increments of $\overline{V}_{max}$, $\overline{R}_{34kt}$, and f to minimize the effect of sample size variability. The bootstrapped 95% confidence interval range on each coefficient is (−7.51, −5.02) for β_0, (−0.0134, −0.0123) for β_{Vmax^2}, (−5.961, −5.122) for β_{fR}, and (96.439, 127.265) for β_{fRdV}.

Model performance is shown in Fig. 1b, which displays predicted [Eq. (5)] versus observed ΔP for the raw dataset shown in Fig. 1a. Equation (5) explains 94.2% of the variance in ΔP_{hPa}, with an RMS error of 5.24 hPa (Table 1). The model is nearly unbiased across the full range of ΔP_{hPa}, as evident by the solid red line (binned median) in Fig. 1b closely following the black one-to-one line. This unbiased behavior extends to the most extreme data points with the largest pressure deficits (lower-left region of the figure).

The sign of the dependence on each parameter matches the theory. First and foremost, the model predicts larger pressure deficit (ΔP_{hPa}) at higher intensity ($\overline{V}^2_{max}$; positive dependence) and at larger size or higher latitude [$(1/2)f\overline{R}_{34kt}$; positive dependence], as has been shown in past work (KZ07; Chavas et al. 2017). The third term is more complex and is new. Given the positive coefficient, it yields a more intense storm (more negative pressure deficit) at higher $\overline{V}_{max}$ or at smaller size or higher latitude (these both would make the

TABLE 1. Model performance for our final MLR model (top line in bold) and alternative versions to test the effect of modifications to the model formulation. See the text for details. Model performance plots analogous to Fig. 1 for each entry are provided in Fig. S01.

Model	Explained variance ($100 \times r^2_{adj}$)	Error [ϵ_{RMS} (hPa)]	MLR model coefficients
Final model [Eq. (5)]	**94.2**	**5.24**	$(\beta_0, \beta_{Vmax^2}, \beta_{fR}, \beta_{fRdV}) = (-6.60, -0.0127, -5.506, +109.013)$
$\overline{V}^2_{max}$ and $(1/2)f\overline{R}_{34kt}$ only	92.3	6.03	$(\beta_0, \beta_{Vmax^2}, \beta_{fR}) = (-2.00, -0.0154, -2.469)$
$\overline{V}^2_{max}$ only	84.6	8.55	$(\beta_0, \beta_{Vmax^2}) = (-13.37, -0.0157)$
$\overline{V}_{max}$ only	88.3	7.43	$(\beta_0, \beta_{Vmax^2}) = (20.23, -1.54)$
Predict P_{min} instead of ΔP	93.3	5.62	$(\beta_0, \beta_{Vmax^2}, \beta_{fR}, \beta_{fRdV}) = (1005.92, -0.0130, -5.022, +107.719)$
Predict $P_{min} = \mathscr{F}(\overline{V}_{max})$ (classic wind–pressure)	89.2	7.13	$(\beta_0, \beta_{Vmax}) = (1035.08, -1.56)$
Include 30°–50°N data	93.5	5.40	$(\beta_0, \beta_{Vmax^2}, \beta_{fR}, \beta_{fRdV}) = (-6.67, -0.0126, -5.462, +105.138)$
No translation modification	94.4	5.21	$(\beta_0, \beta_{Vmax^2}, \beta_{fR}, \beta_{fRdV}) = (-3.37, -0.0128, -4.837, +92.689)$
Nonlinear translation (KZ07)	94.1	5.26	$(\beta_0, \beta_{Vmax^2}, \beta_{fR}, \beta_{fRdV}) = (-6.52, -0.0128, -5.457, +104.956)$
$\overline{V}_{max}$, $\overline{R}_{34kt}$, and f	93.2	5.69	$(\beta_0, \beta_{Vmax^2}, \beta_R, \beta_f) = (36.28, -1.48, -7.10 \times 10^{-5}, -1.21 \times 10^5)$
$\overline{V}^2_{max}$, $\overline{R}_{34kt}$, and f	92.0	6.17	$(\beta_0, \beta_{Vmax^2}, \beta_R, \beta_f) = (6.05, -0.0151, -8.02 \times 10^{-5}, -1.25 \times 10^5)$

term less positive). Hence, this term slightly enhances the dependence on $\overline{V}_{max}$ (first term) but slightly reduces the dependence on $(1/2)f\overline{R}_{34kt}$ (second term). We show below that this new predictor has the smallest effect of the three predictors but still adds value to the model's predictive power.

b. *Tests of model formulation*

We next evaluate the effect of each predictor as well as a few choices made in the formulation of our final model. Changes in model performance for modifications to our model are shown in Table 1. In each case, the alternative model was fit and tested in an identical fashion as was done for our full model above.

First, we remove the least valuable predictor one at a time and present the model results for direct comparison to the full model. Removing the third predictor (ratio) increases the unexplained variance from 5.8% to 7.7%. Further removing the second predictor (size and latitude), i.e., a linear regression on $\overline{V}^2_{max}$ alone, further increases the unexplained variance to 15.4%. Finally, replacing $\overline{V}^2_{max}$ with $\overline{V}_{max}$ partially reduces the unexplained variance back to 11.7%; hence, if using the maximum wind speed alone, $\overline{V}_{max}$ is preferable to $\overline{V}^2_{max}$.

We also tested the same model but using P_{min} rather than ΔP as the predictand (i.e., ignoring variations in P_{env}), which results in a slight reduction of performance with an increase in unexplained variance from 5.8% to 6.7%. This effect is relatively small but does indicate that the knowledge of variations in the environmental pressure can help modestly improve the prediction of P_{min} for a given storm.

Last, we combine the above two tests to examine a standard wind–pressure relationship, i.e., predicting P_{min} from $\overline{V}_{max}$ alone. This leaves 10.8% of the variance unexplained. This model actually performs better than the two models that predict ΔP from $\overline{V}_{max}$ or $\overline{V}^2_{max}$. This result gives insight into why the standard wind–pressure relationship has been so successful, as apparently $\overline{V}_{max}$ may coincidentally capture a bit of the residual variance associated with the other two terms and variations in environmental pressure. Overall, our full model offers a significant improvement in performance over a standard wind–pressure relationship by capturing nearly half of the residual variance in the latter (94.2% vs 89.2% variance explained).

Note that we also tried a range of other model fits with $\overline{V}_{max}$, $\overline{R}_{34kt}$, and f arbitrarily employed in a variety of ways both linearly and nonlinearly. However, none outperformed our theory-driven version presented above. In particular, a straightforward empirical model that takes our input parameters $\overline{V}_{max}$, $\overline{R}_{34kt}$, and f as direct predictors [similar to Courtney and Knaff (2009)] performs slightly worse than our model, adding an additional 1.0% unexplained variance; replacing $\overline{V}_{max}$ with $\overline{V}^2_{max}$ further reduces performance. This does not outright prove that the theory-derived set of parameters found here are the "optimal" parameters, but it does lend confidence that theory really can provide useful guidance on how the observed parameters are best combined for the purposes of predicting the pressure deficit. Clearly, a more standard empirical model is also viable, but our model has the added benefit of being grounded in physics.

Finally, we test two other choices in our model formulation. First, the above outcomes hold true for the model fit to the same dataset but including all cases up to 50°N. Its performance (93.5% variance explained) is slightly degraded relative to our model up to 30°N, which is unsurprising given the greater complexity of cases at higher latitudes. We return to this topic below.

Second, we chose to reduce the best track V_{max} to account for translation speed effects as has been done in the past. The result is very similar when using V_{max} without this translation reduction, with a slight increase of 0.2% in explained variance. However, without a translation speed modification, there exists a strong systematic dependence of model error on V_{trans} that is found in both our primary developmental dataset and when the model is applied to our high-latitude subset [discussed in section 4c(1) below]. Both of these systematic dependencies are eliminated by applying the translation speed modification (see Fig. S02 in the online supplemental material). Moreover, while the inclusion of the translation modification does not improve model performance for our

data below 30°N, it does modestly improve model performance when applied to the high-latitude subset (0.8% increase in explained variance; 0.3-hPa reduction in RMS error). The interpretation of this outcome is that, because V_{trans} tends to vary much more strongly in the subtropics than in the tropics, the translation signal only emerges from the noise of adding an additional input parameter when applied to these higher-latitude cases in isolation. Given that this translation effect on the wind field is widely known to be real (e.g., KZ07) and indeed is apparent in our dataset, it is important to include in our model. We further test a second method from KZ07, originating from Schwerdt et al. (1979), which applies a slightly nonlinear translation modification given by $\overline{V}_{\text{max}} = V_{\text{max}} - 1.5V_{\text{trans}}^{0.63}$. This method yields a very similar result to our linear modification, except that it does not fully eliminate the dependence of model error on V_{trans} for the high-latitude cases (Fig. S02). For the above reasons, we elected to use the simple linear translation modification to V_{max} given by Eq. (2) in our model.

c. *Applications to special subsets*

1) HIGH-LATITUDE STORMS

We next apply our model to the data for high-latitude storms spanning 30°–50°N in our database (Fig. 2). At these higher latitudes, jet stream interactions and the onset of extratropical transition are much more likely, storms tend to expand, and North Atlantic storms often have significant interactions with land to the west. Hence, data in this region are associated with much larger uncertainty in both input parameter estimates $\overline{V}_{\text{max}}$ and $\overline{R}_{34\text{kt}}$ and structural relationships among parameters. Nonetheless, the model performs reasonably well for this generally more complex subset of cases, explaining 87.8% of the variance with an RMS error of 6.0 hPa. The model provides a nearly unbiased estimate of ΔP for values down to −60 hPa. For the deepest storms, though, there is evidence of a systematic overestimation of ΔP. Overall, while the performance is clearly worse than when applied to lower latitude storms as expected, the model appears to extrapolate well to higher latitudes. For further context, the high-latitude case of Hurricane Sandy is explored in the case studies section of this paper.

2) LAND PROXIMITY STORMS

Finally, we apply our model specifically to tropical cyclones that are relatively close to land and hence potentially of greater risk for coastal populations. Land introduces significant asymmetry in the surface wind field that would be expected to increase uncertainty, particularly in the estimation of $\overline{R}_{34\text{kt}}$. Results for our model application to all data within 200 km of a coastline up to 50°N are shown in Fig. 3. Model performance is again quite strong, explaining 93.3% of the variance with an RMS error of 6.10 hPa and is nearly unbiased over the full range of pressure deficits. The error spread increases for stronger storms with pressure deficits <−60 hPa relative to weaker storms in this subset as well as comparable storms in our full dataset. Overall, though, the model also applies well for storms that are close to land.

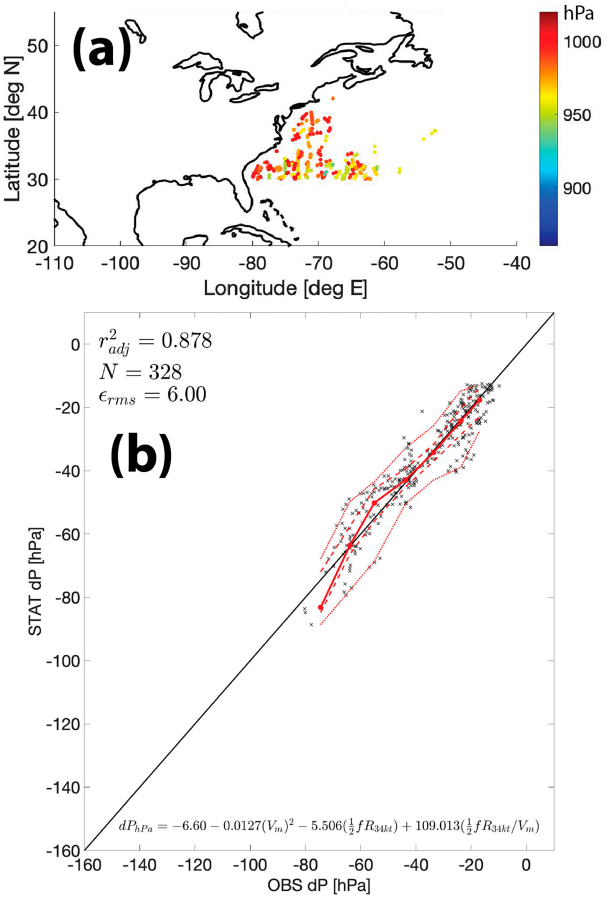

FIG. 2. As in Fig. 1, but for ΔP predicted by our final model [Eq. (5)] for data between 30° and 50°N.

d. *Practical application: extended best track and historical case studies*

We next demonstrate how the model can be put into direct practical use to predict P_{min} using only operationally available data. We use data exclusively from the EBTRK database (2004–22), which provides all parameters that are estimated in near–real time and are later refined in postseason best tracking. Translation speed is again defined from the change in storm center latitude and longitude during the preceding 12 h. We apply the model to the North Atlantic only to give a more apples-to-apples comparison to our observation-based dataset that is weighted heavily toward the North Atlantic.

The lone parameter from our original analysis that was not already routinely estimated is the environmental pressure P_{env}, which is needed to translate the model's prediction for ΔP back into P_{min}. In our prior analyses, we had estimated P_{env} from the pressure field in global model reanalysis, which is more precise but not operationally available. Here, we utilize the pressure of the outermost closed isobar (P_{oci}) and apply a simple constant offset

$$P_{\text{env}} = P_{\text{oci}} + 2\,\text{hPa}. \tag{6}$$

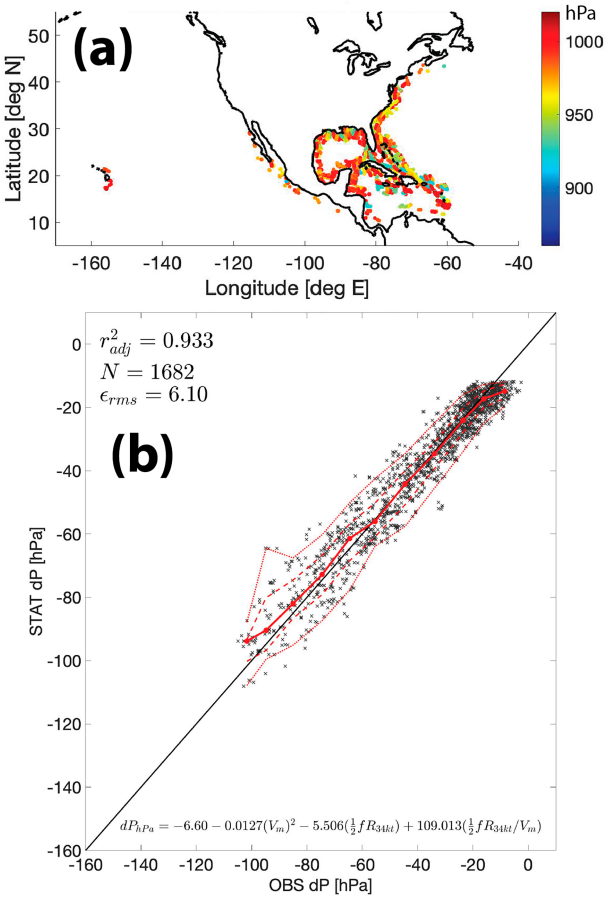

FIG. 3. As in Fig. 1, but for ΔP predicted by our final model [Eq. (5)] for data close to land, defined as within 200 km of a coastline.

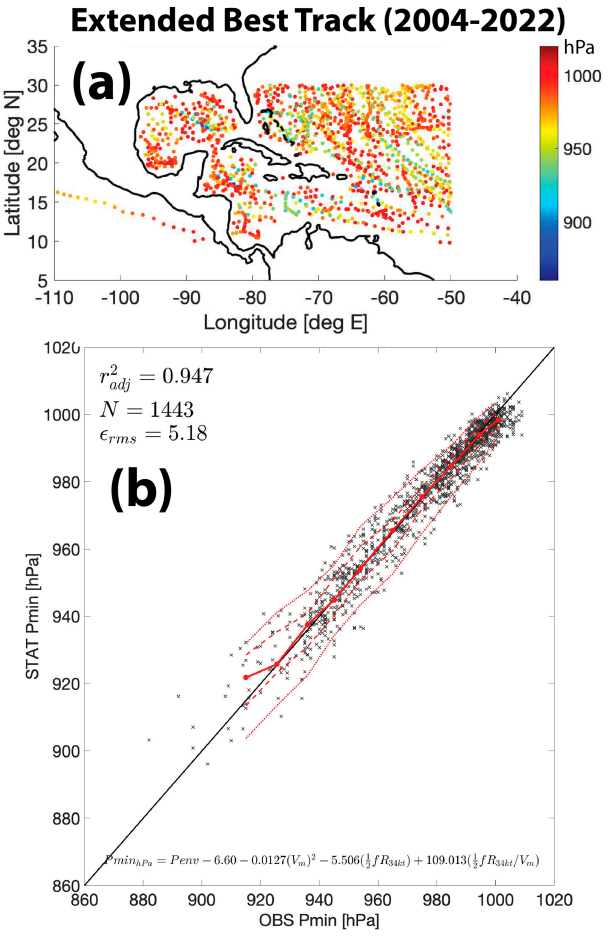

FIG. 4. As in Fig. 1, but for the "operational" model prediction, with ΔP predicted by our final model [Eq. (5)] using only the EBTRK database for the period 2004–22 in the North Atlantic for all data and P_{env} estimated from P_{oci} using Eq. (6).

The value of 2 hPa was estimated directly from our model by finding the value that eliminates the mean bias in our prediction (an increase/decrease in P_{env} simply acts to increase/decrease P_{min} by the same amount). As shown below, this offset results in a near-zero conditional bias across all values of P_{min}, which indicates that using a simple constant for an offset is reasonable. Notably, this estimate of P_{env} agrees with recommendations in Courtney and Knaff (2009).

We predict P_{min} by calculating ΔP using Eq. (5) and P_{env} using Eq. (6). The results are shown in Fig. 4. The prediction compares quite well with the EBTRK data, explaining 94.7% of the variance with an RMS error of 5.18 hPa. The performance is very similar to that found above using the observation-based database. This is to be expected, as EBTRK should mostly be very similar to our database, with the exception of EBTRK being at a 6-hourly temporal resolution and for occasional times when aircraft reconnaissance was not available, which should be relatively infrequent by design given our focus on the western Atlantic.

These results indicate that one can make a good prediction for P_{min} if given high-quality operational estimates of $\overline{V}_{max}$, $\overline{R}_{34kt}$, storm-center latitude, and pressure of the outermost closed isobar. This may be of direct value when remote sensing–based wind speed measurements are available but measurements of P_{min} are not.

HISTORICAL CASE STUDIES

Last, we illustrate our model applied to case studies of five impactful historical hurricanes: Patricia (2015), Ike (2008), Rita (2005), Michael (2018), and Sandy (2012) in Fig. 5. The cases are presented roughly in order from least complex to most complex in terms of life cycle evolution. We again compare our model by calculating ΔP using Eq. (5) and P_{env} using Eq. (6) using extended best track data. Overall, our model does reasonably well to predict P_{min} across all five cases, but it is insightful to discuss both successes and notable biases across the cases.

Patricia (2015; Figs. 5a–c) was a category 5 storm in the eastern North Pacific that made landfall in Jalisco in western Mexico as a category 4 hurricane (Fig. 5a). Patricia was the most intense hurricane on record based on $\overline{V}_{max}$ and exhibited the fastest rate of 24-h intensification on record

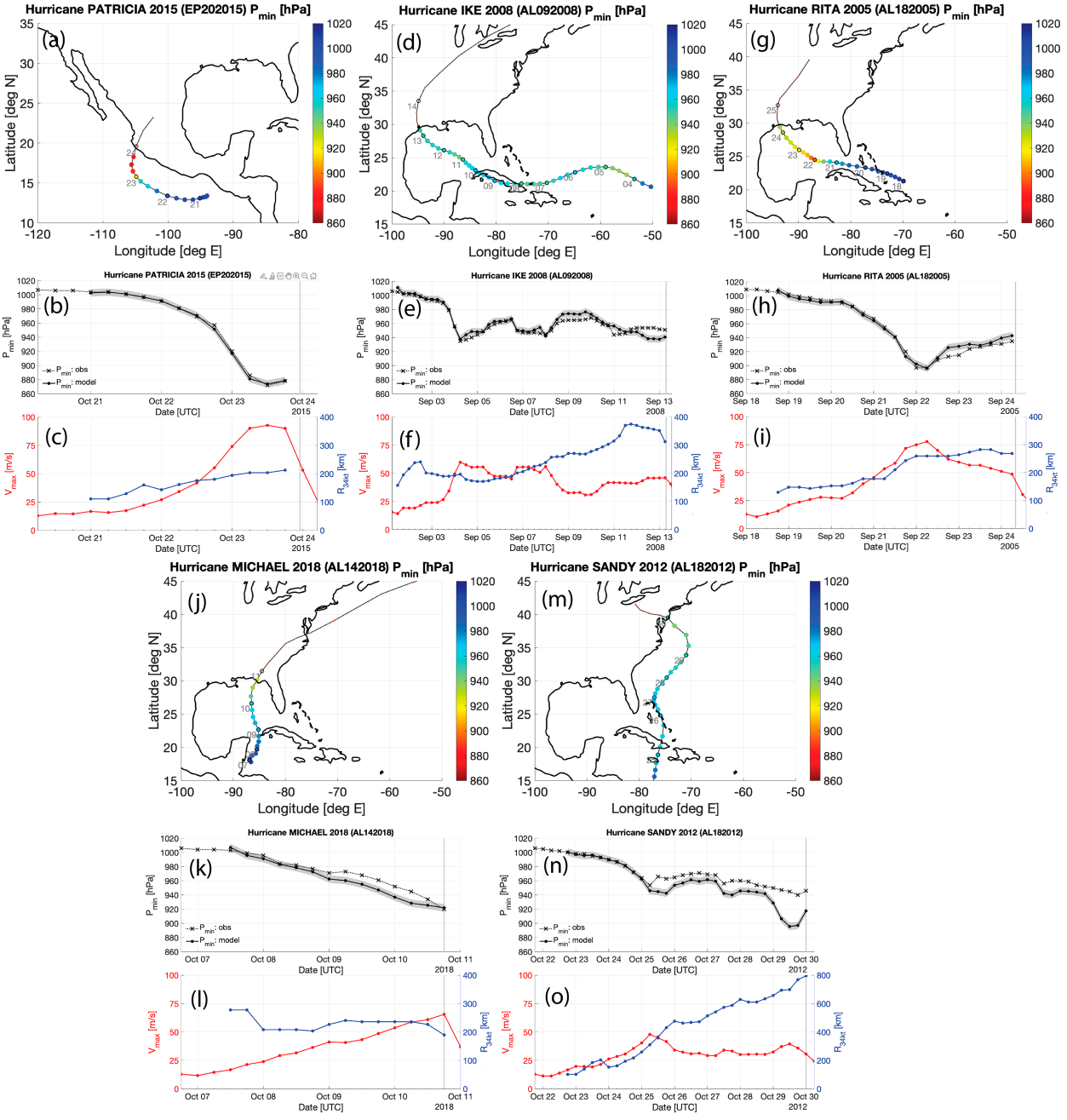

FIG. 5. Model prediction for five case studies of recent impactful storms. Patricia (2015, EP): (a) map of track and $P_{\min}$ (color); (b) time series of best track $P_{\min}$ vs model prediction from best track operational inputs only; (c) maximum wind speed ($\overline{V}_{\max}$) and mean radius of 34-kt wind ($\overline{R}_{34\mathrm{kt}}$). Identical analyses for (d)–(f) Ike (2008, AL); (g)–(i) Rita (2005, AL); (j)–(l) Michael (2018, AL); and (m)–(o) Sandy (2012, AL). Note the change in scale for $\overline{R}_{34\mathrm{kt}}$ for Sandy in (o). The vertical gray line in each time series denotes the time of CONUS landfall. The gray band represents an error of ±5.18 hPa, which is the model RMSE error of Fig. 4. Date labels on the map correspond to 0000 UTC.

(Kimberlain et al. 2016). Hence, it represents an excellent test case for extreme maximum wind speeds for our model. Our model does a remarkably good job of predicting the minimum pressure throughout its entire life cycle (Fig. 5b). The model exhibits a near-zero error during its initial period of intensification through 1200 UTC 22 October as well as at its peak intensity (lowest pressure) at 1200 UTC 23 October, with a modest high bias of approximately +5 hPa during the intervening 18 h of very rapid intensification. In this case, the evolution of $P_{\min}$ is driven almost entirely by $\overline{V}_{\max}$, as size ($\overline{R}_{34\mathrm{kt}}$) increases only

very gradually with time (Fig. 5c). Additionally, Patricia remained at a relatively constant latitude, moving poleward by only 5° prior to landfall.

Ike (2008; Figs. 5d–f) was a category 4 storm in the North Atlantic that made multiple landfalls along the coasts of the Turks and Caicos Islands, Cuba, and finally Texas (Fig. 5d). Ike grew substantially in size throughout its life cycle while its intensity fluctuated (Fig. 5f) and hence is a good test case of a storm that exhibited significant variations in both intensity and size. Our model does an excellent job of predicting the evolution of P_{min} (Fig. 5e). The model had a high bias (too weak) of approximately +10 hPa from 1800 UTC 8 September to 0600 UTC 11 September, a period during which Ike was passing along the long axis of Cuba. Note that many of those data occurred when the storm center was just offshore but close enough that the inner core of the storm almost certainly was partially onshore resulting in strong interaction with land (Berg 2009); the complexity of this interaction likely explains the discrepancy during that period. Thereafter, an eyewall replacement cycle occurred on 10 September that corresponded with a period of significant expansion through 1200 UTC 11 September while the maximum wind speed remained steady. At 0000 UTC 11 September, the minimum pressure dropped and then increased very slowly to 950 hPa through 1200 UTC, whereas our model predicted a more gradual decrease in pressure during this period. Finally, through landfall at 0600 UTC 13 September, the observed minimum pressure remained relatively constant, hovering within 5 hPa of its final landfall pressure along Galveston Island, Texas, of 950 hPa. Our model, on the other hand, predicted a continued decrease in minimum pressure due to the slight intensification during 0000–0600 UTC 12 September combined with its gradual poleward movement. Given the storm's very large size as it approached land, there is likely greater uncertainty in the estimate of $\overline{R}_{34kt}$ in the model, which may explain the discrepancy during this period.

Rita (2005; Figs. 5g–i) was a category 5 storm in the North Atlantic that followed a very similar track as Ike through the northern Caribbean and Gulf of Mexico, except shifted slightly northward such that it passed through the Straits of Florida to the north of Cuba rather than directly over Cuba (Fig. 5g). Rita also expanded steadily after interacting with Cuba. In contrast to Ike, during this expansion period, Rita intensified rapidly, from 0000 UTC 21 September through 0000 UTC 22 September (Fig. 5i). The final combination of extreme intensity and large size yielded the lowest Atlantic P_{min} on record for the Gulf of Mexico (895 hPa). Our model performed very well over most of Rita's life cycle (Fig. 5h), including a near-zero bias through the period of intensification and expansion and at peak intensity from 0000 to 0600 UTC 22 September. Thereafter, our model briefly exhibited a moderate high bias from 1800 UTC 22 September through 0000 UTC 23 September and then performed well with a smaller bias of 5–10 hPa leading up to landfall. The landfall pressure of 937 hPa was the lowest on record in the Atlantic basin for an intensity of 100 kt (Knabb et al. 2006), owing to its large size. Note that Rita's landfall intensity was slightly higher than Ike (100 vs 95 kt), but Rita was also slightly smaller than Ike. Rita's landfall pressure was lower than Ike's landfall pressure, whereas our model predicted the opposite. Hence, the model had a low bias for Ike and a high bias for Rita at landfall. Similar to Ike, Rita's large size as it approached land likely created larger uncertainty in the value of $\overline{R}_{34kt}$. Overall, Rita and Ike demonstrate how, for larger storms, size contributes significantly to reducing the minimum pressure relative to what would be expected from the maximum wind speed alone. Rita and Ike made landfall at very similar latitudes (29.7°N for Rita and 29.3°N for Ike), so Coriolis played effectively no role in the differences between these two storms at landfall. As noted at the start of the introduction, these large hurricanes with low P_{min} relative to best track V_{max} can cause confusion when considering how to communicate the severity of a storm, which is especially problematic when approaching land.

Michael (2018; Figs. 5j–l) was a category 5 storm in the North Atlantic that made landfall in the Florida Panhandle at its peak intensity of 140 kt. The system moved north throughout its life cycle prior to landfall from its genesis location in the far western Caribbean (Fig. 5j). Michael was similar to Patricia in that it reached extreme intensities while its size remained relatively constant, but it did so by intensifying more gradually and uniformly over a 4-day period leading up to landfall (Fig. 5l). Our model did very well in predicting the continuous decrease in P_{min} with time, particularly over its first few days prior to 0000 UTC 9 October during which the model had a near-zero error (Fig. 5k). Our model then exhibited a moderate low bias (too intense) from −10 to 15 hPa during the final 2 days leading up to landfall, with the error returning to near zero just prior to landfall. At 1800 UTC 8 October, Michael passed very close to the western tip of Cuba and thereafter experienced a decay in its eyewall structure (Beven et al. 2019). This interaction with land may have induced uncertainties in wind radii estimates and changes in Michael's structure that were not captured by our model.

Finally, Sandy (2012; Figs. 5m–o) was a highly destructive storm in the North Atlantic that became the largest storm ever recorded in the basin as measured by $\overline{R}_{34kt}$. Sandy made multiple landfalls in Jamaica, Cuba, and finally New Jersey as a posttropical cyclone 2.5 h after completing extratropical transition (Fig. 5m). Sandy represents perhaps the most complex of test cases, with dramatic changes in intensity, size, and latitude throughout its life cycle (Fig. 5o), multiple sustained interactions with land, and substantial extratropical interactions. Our model does well in predicting P_{min} during its early stages in the southern Caribbean prior to crossing Cuba at 0600 UTC 25 October (Fig. 5n). From 1200 UTC 25 October through 1800 UTC 26 October, our model exhibited a moderate low bias (too intense) from −10 to −20 hPa, particularly as the storm center crossed Cuba and then subsequently moved along the axis of the Turks and Caicos and the Bahamas. This period of time was associated with a sharp leveling off and then a decrease in $\overline{V}_{max}$ concurrent with a very rapid expansion in storm size. This expansion was driven by the strong interaction with an upper-level trough and later a warm frontal boundary, which resulted in the development of an unusual structure with an exceptionally large R_{max}, and the

strongest winds found on the western semicircle (Blake et al. 2013). The model performed better from 0000 to 1200 UTC 27 October before the bias increased again to −15 hPa as Sandy moved back out over the open water while rapidly undergoing extratropical transition. Sandy was formally designated as an extratropical system on 2100 UTC 29 October as the storm approached the New Jersey coastline, and indeed our model exhibited a very large low bias (far too intense) during 29 October, predicting a minimum pressure below 900 hPa when the actual value was 940 hPa prior to landfall. Hence, Sandy demonstrates how our model may not be well suited for storms that have undergone substantial extratropical transition, for which the assumptions regarding the radial structure of the winds may break down. However, it is also worth noting that the estimation of the input parameter values ($\overline{V}_{\max}$ and $\overline{R}_{34\mathrm{kt}}$) is likely highly uncertain during this latter period given that Sandy was a large and highly asymmetric storm whose wind field significantly overlapped with the adjacent land.

Note that the biases in the above cases, particularly Ike and Michael, tend to be persistent for periods of 1–2 days when they occur. Such biases may be driven by a variety of factors. Estimating $R_{34\mathrm{kt}}$ for larger storms may be more uncertain given that aircraft observations extend only 200 km from the center, so estimates depend more strongly on scatterometry data and can only be updated when new data become available. Land interaction may induce low biases in size as noted above. Additionally, there is uncertainty in estimating the environmental pressure P_{env} from P_{oci}, as the closure of isobars depends on the synoptic-scale atmospheric flow on the periphery of the storm that tends to vary more slowly in time. Evaluating the relative role of uncertainties lies beyond the scope of this work. Future work might seek to develop more precise estimates of the environmental pressure, such as our method used above based on global analyses, that can be used both in an operational setting and in the best track archive.

5. Conclusions

A simple model to predict $P_{\min}$ in a tropical cyclone from routinely estimated data would be useful for operations and practical applications. This work has developed an empirical linear model for the pressure deficit that takes as input the maximum wind speed, the mean radius of 34-kt wind, and storm central latitude, as well as the environmental pressure. The specific model predictors, given by $\overline{V}^2_{\max}$, $(1/2)fR_{34\mathrm{kt}}$, and the ratio of the latter to the former, are derived from gradient wind balance applied to a modified Rankine vortex. Rather than using the full analytic solution itself, which will bake in the approximating assumptions of the theory, we instead use a simple linear regression model on those three parameters and estimate the coefficients from historical data: aircraft-estimated central pressure, historical best track data for storm wind field parameters, and global analyses for environmental pressure. This choice enables us to exploit the unique benefits of both physical theory (predictors) and data (dependence on predictors). The model shows excellent skill, capturing 94.4% of the variance in the historical dataset and outperforming various other versions of the model. It is superior to a standard wind–pressure relationship (89.4% variance explained), which indicates that the inclusion of size and latitude information captures approximately half of the residual variance that is unexplained by this simpler model. Though the model was fit to data over the open ocean in the tropics in order to minimize the effects of observational uncertainties, it also appears to perform well at high latitudes and near coastlines. Finally, it performs very well when applied solely using data from the extended best track database (94.9% variance explained), which indicates it is viable in an operational setting using only routinely estimated data.

The final model for the pressure deficit is given by Eq. (5). The pressure deficit prediction is then translated to a prediction for $P_{\min}$ via Eq. (3) by adding an estimate of the environmental pressure, which may be estimated operationally using the pressure of the outermost closed isobar via Eq. (6).

Overall, this simple and fast model can predict $P_{\min}$ from maximum wind speed, storm size, storm central latitude, and environmental pressure in practical applications. In operations, the model could give a preliminary estimate of $P_{\min}$ if other input predictors are available. Perhaps more importantly, $P_{\min}$ can potentially be forecast up to 5 days from the operational forecast time in the North Atlantic and eastern North Pacific given that the National Hurricane Center forecasts $V_{\max}$ and storm central position operationally out to 120 h and in 2024 will begin doing so for 34-kt wind radii as well. Currently, the National Hurricane Center does not operationally forecast $P_{\min}$, but this simple tool would allow for a simple estimate of $P_{\min,}$ which would not entail additional work for the forecaster on duty. This information combined with a radius of maximum wind estimates using similar methods (Chavas and Knaff 2022; Avenas et al. 2023) could particularly be useful for storm surge model initial conditions.

In risk analysis, the model can help provide mutually consistent estimates of these three parameters that extend to other/future climate states where no observational data exist. In weather and climate modeling, the model could provide a new tool to evaluate the representation of TC intensity, size, and $P_{\min}$ jointly, as well as to understand how future changes in $P_{\min}$ reflect changes in intensity versus size. More broadly, given the strong correlation between $P_{\min}$ and historical economic damage, the model offers a full quantitative bridge from the wind field to hazards to damage that may be of use in the study of damage risk in both real-time forecasting and under climate change. Moreover, this model can help explain why larger storms can make it difficult to communicate the potential severity of a storm when $P_{\min}$ is substantially lower than expected for a given maximum wind speed (and the Saffir–Simpson hurricane wind scale category) based on a standard wind–pressure relationship.

We note that improved parameter estimation, particularly of $R_{34\mathrm{kt}}$ and of the environmental pressure, may both help improve model performance for individual cases. As this method relies on operational estimates of $V_{\max}$, $R_{34\mathrm{kt}}$, and P_{env}, any improvements in those estimates will help in predicting $P_{\min}$. Our estimates of P_{env} can certainly be improved by more direct methods using global model analyses. Uncertainties

associated with V_{max} and R_{34kt} are on the order of 5 m s^{-1} and 26 km, respectively (Torn and Snyder 2012; Sampson et al. 2017; Combot et al. 2020), which will likely persist as a few observational platforms exist that accurately estimate R_{34kt} and V_{max} (Knaff et al. 2021). Additionally, recent work has shown that satellite-based Dvorak current intensity estimates could be used in lieu of maximum wind speed to predict the minimum pressure (Aizawa et al. 2024), which is a viable alternative in the absence of direct observations of the maximum wind speed.

Finally, we note that this model provides a physical explanation for how the TC minimum pressure is expected to change with global warming. On average, we expect tropical cyclones in a warmer world to become more intense (higher maximum wind speed; Knutson et al. 2020; Emanuel 1987, 2021) at a relatively constant outer size (Knutson et al. 2015; Schenkel et al. 2023; Stansfield and Reed 2021; Lu and Chavas 2022) and a relatively constant latitude with the exception of a slow expansion of the poleward edge of TC activity (Kossin et al. 2014). Environmental pressures would not be expected to change significantly. Taken together, our model would then predict lower central pressures, driven by the increase in maximum wind speed, consistent with modeling studies (Knutson et al. 1998; Kanada et al. 2013; Tran et al. 2022). Additionally, based on the simple modified Rankine vortex that underlies our model, the radial structure of the wind field would be expected to remain constant with the exception of a slight contraction of the radius of maximum wind at higher intensities, as is found in observations and modeling studies (Chavas and Lin 2016; Kanada et al. 2013; Tran et al. 2022; Chen et al. 2022). Hence, the physical basis of the model provides a pathway to link changes in different aspects of tropical cyclone structure and to more confidently extrapolate to other climate states for which we do not have direct observations.

Acknowledgments. D. R. Chavas acknowledges funding support from NSF AGS Grant 1945113. P. Klotzbach acknowledges funding support from the G. Unger Vetlesen Foundation. J. A. Knaff thanks his employer, NOAA/Center for Satellite Applications and Research, for supporting this work. The scientific results and conclusions, as well as any views or opinions expressed herein, are those of the author(s) and do not necessarily reflect those of NOAA or the Department of Commerce.

Data availability statement. Data and code for this work are publicly available via the Purdue University Research Repository (PURR) at http://doi.org/doi:10.4231/GSVZ-D752 (Chavas 2025).

APPENDIX

Derivation of Theoretical Pressure Deficit Model

Here, we derive the analytic solution for the pressure deficit ΔP at the center of the storm that yields the three physical parameters used in the model presented in the main text. Klotzbach et al. (2022) showed that a modified Rankine model well reproduces the relationship between R_{max} and R_{64kt}, R_{50kt}, and particularly $\overline{R}_{34kt}$ in the EBTRK database over the tropical western Atlantic. This empirical outcome combined with the analytic simplicity of a modified Rankine wind profile motivates its use below.

The pressure deficit relative to a fixed radius can be expressed using gradient wind balance (KZ07; Chavas et al. 2017), given by

$$\Delta P = -\int_0^{R_o} \rho\left(\frac{v^2}{r} + fv\right)dr, \tag{A1}$$

where ρ is the air density, v is the rotating wind speed, f is the Coriolis parameter at the storm center and ϕ is the latitude of the storm center, r is radius ($r = 0$ is the storm center), and R_o is some larger radius. The term ΔP is defined as negative when the pressure decreases moving inwards, such that a stronger storm will have a more negative pressure deficit.

If given a profile of v as a function of radius, Eq. (A1) can predict how pressure decreases moving inwards toward the center, including the total pressure deficit. A simple model for the wind profile inside of $\overline{R}_{34kt}$ makes use of the modified Rankine equation:

$$\frac{v}{\overline{V}_{max}} = \left(\frac{r}{R_{max}}\right)^{\alpha}, \tag{A2}$$

where $\overline{V}_{max}$ is the azimuthal-mean maximum wind speed and R_{max} is the radius of maximum wind. In the eye region ($r \le R_{max}$), we take $\alpha_e = 2$, i.e., a parabola. Outside of the eye region ($r \ge R_{max}$), we take $\alpha_o = -0.5$, which is close to the best-fit value of -0.55 estimated from extended best track data in the southwest Atlantic Ocean shown in Fig. 8a of Klotzbach et al. (2022). An example of the pressure deficit profile calculated numerically from this wind profile using Eq. (A1) at $\phi = 20°$N is shown in Fig. A1.

The simplicity of the wind model allows one to directly derive an analytic solution for ΔP by combining Eqs. (A1) and (A2). To do so, it is helpful to first write Eq. (A1) in terms of $\tilde{v} = v/\overline{V}_{max}$ and $\tilde{r} = r/R_{max}$, since the wind model [Eq. (A2)] is also written in this form, i.e.,

$$\tilde{v} = \tilde{r}^{\alpha}. \tag{A3}$$

We further take ρ to be constant. Doing so yields

$$\Delta P = \rho \overline{V}_{max}^2 \left(\int_0^{\tilde{R}_o} \frac{\tilde{v}^2}{\tilde{r}} d\tilde{r} + f\int_0^{\tilde{R}_o} \tilde{v}\, d\tilde{r}\right), \tag{A4}$$

where $\tilde{R}_o = R_o/R_{max}$. Using Eqs. (A3) and (A4), ΔP can be calculated analytically both within the eye region (ΔP_e; $\tilde{r} < 1$) and outside the eye region (ΔP_o; $\tilde{r} > 1$), with the total pressure deficit equal to the sum of the two:

$$\Delta P = \Delta P_e + \Delta P_o. \tag{A5}$$

The general solution for any α is given by

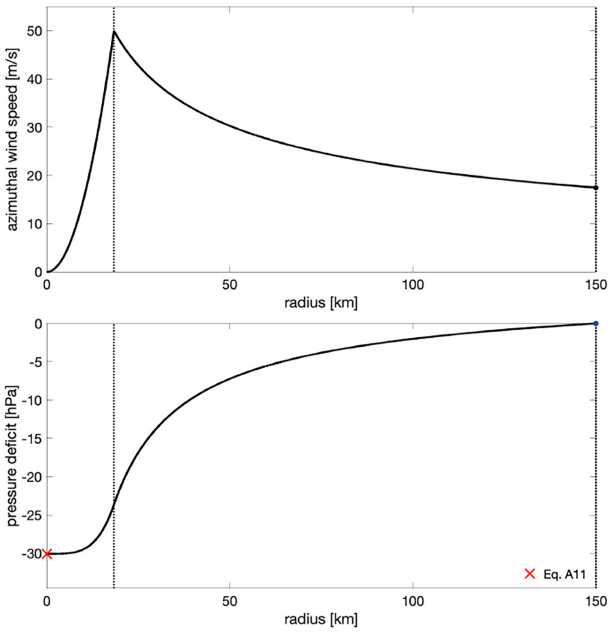

FIG. A1. Example calculation of the pressure deficit ΔP inside of $\overline{R}_{34\mathrm{kt}}$ for the wind profile used in this study based on a modified Rankine structure, $v/\overline{V}_{\max} = (r/R_{\max})^{\alpha}$. (a) Wind profile, with $\alpha_e = 2$ in the eye ($r \le R_{\max}$) and $\alpha_o = -0.5$ outside of the eye ($r \ge R_{\max}$); (b) pressure deficit profile calculated from gradient wind balance and prediction from Eq. (A11) (red x), with density assumed constant at $\rho = 1$ kg m^{-3}.

$$\Delta P_e = -\left(\frac{\rho}{2\alpha_e}\right)\overline{V}_{\max}^2 - \left[\frac{2\rho}{(\alpha_e + 1)V_o^{1/\alpha_o}}\right]\left(\frac{1}{2}fR_o\right)\overline{V}_{\max}^{1+(1/\alpha_o)} \quad \text{(A6)}$$

within the eye and

$$\Delta P_o = -\left(\frac{\rho}{2\alpha_o}\right)(V_o^2 - \overline{V}_{\max}^2) - \left[\frac{2\rho}{(\alpha_e + 1)V_o^{1/\alpha_o}}\right]\left(\frac{1}{2}fR_o\right) \times [V_o^{1+(1/\alpha_o)} - \overline{V}_{\max}^{1+(1/\alpha_o)}] \quad \text{(A7)}$$

within the outer region. We plug in $\alpha_e = 2$ and take $\alpha_o = -0.5$, which is close to the best estimate of -0.55 and makes the math for the final solution much simpler. Doing so yields

$$\Delta P_e = -\frac{1}{4}\rho\overline{V}_{\max}^2 - \frac{2}{3}\rho V_o^2\left(\frac{\frac{1}{2}fR_o}{\overline{V}_{\max}}\right) \quad \text{(A8)}$$

within the eye and

$$\Delta P_o = -\rho\overline{V}_{\max}^2 + \rho V_o^2 - 4V_o\left(\frac{1}{2}fR_o\right) + 4V_o^2\left(\frac{\frac{1}{2}fR_o}{\overline{V}_{\max}}\right) \quad \text{(A9)}$$

within the outer region. Adding the two together and combining like terms yields a final equation for the total pressure deficit:

$$\Delta P_{\mathrm{theo}} = \rho\left[V_0^2 - \frac{5}{4}(\overline{V}_{\max}^2) - 4V_o\left(\frac{1}{2}fR_o\right) + \frac{10}{3}V_o^2\left(\frac{\frac{1}{2}fR_o}{\overline{V}_{\max}}\right)\right]. \quad \text{(A10)}$$

This equation is a linear function of three predictors: $\overline{V}_{\max}^2$, $(1/2)fR_o$, and $(1/2)fR_o/\overline{V}_{\max}$. Physically, the first two terms on the right-hand side represent the cyclostrophic pressure drop from R_o to the storm center, and the third and fourth terms represent the size-dependent Coriolis pressure drop from R_o to the storm center. The fourth term has a positive sign, and as a result, it enhances the pressure drop from $\overline{V}_{\max}^2$ (the term is less positive at larger $\overline{V}_{\max}$), and it opposes the pressure drop from $(1/2)fR_o$ (the term is more positive at larger R_o or f). Its physical interpretation is more complicated, as it combines the Coriolis pressure drop within the eye [final term of Eq. (A8), which is negative] with the Coriolis pressure drop inside of $R_{\max}$ that is implicitly *excluded* via the inner limit of integration of the outer model [final term of Eq. (A9), which is positive]. The predictor $(1/2)fR_o/\overline{V}_{\max}$ represents an inverse vortex Rossby number, where $\mathrm{Ro} = \overline{V}_{\max}/(fR_{\max})$ is the Rossby number at $R_{\max}$ but where the modified Rankine vortex effectively allows for $R_{\max}$ to be substituted with R_o. In the wind model presented above, for a given R_o, $R_{\max}$ contracts inwards as $\overline{V}_{\max}$ increases, as is commonly seen in observations (Chavas and Lin 2016). As a result, the eye model is compressed inwards, while the outer region model is extended farther inwards to smaller radii. In doing so, there is a reduction in the Coriolis pressure drop within the eye [final term in Eq. (A8) becomes less negative] and an increase in the Coriolis pressure drop outside of the eye [final term in Eq. (A9) becomes less positive]; the latter is larger in magnitude, yielding a positive combined final term in Eq. (A10). Thus, for higher $\overline{V}_{\max}$ at fixed R_o, this final term becomes less positive, thereby enhancing the pressure drop.

Practically, the first term (ρV_0^2) and the coefficients of the three predictor terms in Eq. (A10) are constants. The three predictors are composed of parameters that are routinely estimated operationally. Note that the model predicts specifically that ΔP is larger in magnitude (more negative) for larger $\overline{V}_{\max}^2$ and $(1/2)fR_o$, but it is smaller in magnitude for larger $(1/2)fR_o/\overline{V}_{\max}$. Taking $V_o = 17.5$ m s^{-1} (i.e., 34 kt), corresponding to $R_o = \overline{R}_{34\mathrm{kt}}$, setting $\rho = 1$ kg m^{-3}, and dividing through by 100 to convert to hectopascal yields

$$\Delta P_{\mathrm{hPa,theo}} = 3.0625 - 0.0125(\overline{V}_{\max}^2) - 0.70\left(\frac{1}{2}f\overline{R}_{34\mathrm{kt}}\right) + 10.208\left(\frac{\frac{1}{2}f\overline{R}_{34\mathrm{kt}}}{\overline{V}_{\max}}\right). \quad \text{(A11)}$$

Why use the empirical model of Eq. (4) rather than directly using Eq. (A11)? Three reasons are as follows:

1) The value $\alpha_o = -0.5$ approximates the best-fit value of -0.55 to simplify the math.

2) The derivation neglects the small pressure drop outside of $\overline{R}_{34kt}$.
3) The derivation assumed constant density in order to be analytically tractable. That is not true though since P decreases with radius while temperature remains relatively constant (Emanuel 1986), and hence density decreases moving radially inwards following the ideal gas law.
4) The model assumes winds are taken at the boundary layer top, which is very difficult to estimate or even agree on a definition in practice. Real data for intensity and size are estimates near the surface. A wind speed reduction due to friction within the boundary layer will reduce wind speeds and hence will low-bias the pressure deficit, but accounting for this is very complex.

Given these assumptions, it is preferable to use the theory solely to identify the most important physical parameters while allowing the empirical model to determine the dependencies (i.e., regression coefficients) found in nature, similar to the approach of Chavas and Knaff (2022) and Avenas et al. (2023) for the radius of maximum wind. The coefficient value for the intensity term is very similar to that found empirically. The coefficient values for the final two terms are both quite a bit smaller in magnitude than what is found empirically (the effects of which would tend to offset one another owing to their opposite signs), indicating that theory would be biased in capturing the precise nature of each of those dependencies. The value of the constant term is slightly positive in the theoretical model but slightly negative in the empirical model, which suggests a deeper pressure drop than predicted by theory. One simple possible explanation is that this difference represents the small pressure drop between $\overline{R}_{34kt}$ and the outer edge of the storm that is neglected in the theory above.

REFERENCES

Aizawa, M., K. Ito, and U. Shimada, 2024: Revisiting Koba's relationship to improve minimum sea-level pressure estimates of western North Pacific tropical cyclones. *J. Meteor. Soc. Japan*, **102**, 377–390, https://doi.org/10.2151/jmsj.2024-018.

Atkinson, G. D., and C. R. Holliday, 1977: Tropical cyclone minimum sea level pressure/maximum sustained wind relationship for the western North Pacific. *Mon. Wea. Rev.*, **105**, 421–427, https://doi.org/10.1175/1520-0493(1977)105<0421:TCMSLP>2.0.CO;2.

Avenas, A., A. Mouche, P. Tandeo, J.-F. Piolle, D. Chavas, R. Fablet, J. Knaff, and B. Chapron, 2023: Reexamining the estimation of tropical cyclone radius of maximum wind from outer size with an extensive synthetic aperture radar dataset. *Mon. Wea. Rev.*, **151**, 3169–3189, https://doi.org/10.1175/MWR-D-23-0119.1.

Bakkensen, L. A., and R. O. Mendelsohn, 2016: Risk and adaptation: Evidence from global hurricane damages and fatalities. *J. Assoc. Environ. Resour. Econ.*, **3**, 555–587, https://doi.org/10.1086/685908.

Berg, R., 2009: Tropical cyclone report: Hurricane Ike (AL092008), 1–14 September 2008. NHC Tech. Rep., 55 pp., https://www.nhc.noaa.gov/data/tcr/AL092008_Ike.pdf.

Beven, J. L., II, R. Berg, and A. Hagen, 2019: Tropical cyclone report: Hurricane Michael (AL142018), 7–11 October 2018. NHC Tech. Rep., 86 pp., https://www.nhc.noaa.gov/data/tcr/AL142018_Michael.pdf.

Blake, E. S., T. B. Kimberlain, R. J. Berg, J. P. Cangialosi, and J. L. Beven II, 2013: Tropical cyclone report: Hurricane Sandy (AL182012), 22–29 October 2012. NHC Tech. Rep., 157 pp., https://www.nhc.noaa.gov/data/tcr/AL182012_Sandy.pdf.

Chavas, D. R., 2025: Code and data for Chavas Knaff Klotzbach (2025) A simple model for predicting tropical cyclone minimum central pressure from intensity and size. Purdue University Research Repository, https://doi.org/10.4231/GSVZ-D752.

——, and N. Lin, 2016: A model for the complete radial structure of the tropical cyclone wind field. Part II: Wind field variability. *J. Atmos. Sci.*, **73**, 3093–3113, https://doi.org/10.1175/JAS-D-15-0185.1.

——, and J. A. Knaff, 2022: A simple model for predicting the tropical cyclone radius of maximum wind from outer size. *Wea. Forecasting*, **37**, 563–579, https://doi.org/10.1175/WAF-D-21-0103.1.

——, K. A. Reed, and J. A. Knaff, 2017: Physical understanding of the tropical cyclone wind-pressure relationship. *Nat. Commun.*, **8**, 1360, https://doi.org/10.1038/s41467-017-01546-9.

Chen, J., C. Y. Tam, Z. Wang, K. Cheung, Y. Li, N.-C. Lau, and D.-S. D. Lau, 2022: Future thermodynamic impacts of global warming on landfalling typhoons and their induced storm surges to the Pearl River delta region as inferred from high-resolution regional models. *J. Climate*, **35**, 4905–4926, https://doi.org/10.1175/JCLI-D-21-0436.1.

Combot, C., A. Mouche, J. Knaff, Y. Zhao, Y. Zhao, L. Vinour, Y. Quilfen, and B. Chapron, 2020: Extensive high-resolution synthetic aperture radar (SAR) data analysis of tropical cyclones: Comparisons with SFMR flights and best track. *Mon. Wea. Rev.*, **148**, 4545–4563, https://doi.org/10.1175/MWR-D-20-0005.1.

Courtney, J., and J. A. Knaff, 2009: Adapting the Knaff and Zehr wind-pressure relationship for operational use in tropical cyclone warning centres. *Aust. Meteor. Oceanogr. J.*, **58**, 167–179, https://doi.org/10.22499/2.5803.002.

DeMaria, M., J. A. Knaff, R. Knabb, C. Lauer, C. R. Sampson, and R. T. DeMaria, 2009: A new method for estimating tropical cyclone wind speed probabilities. *Wea. Forecasting*, **24**, 1573–1591, https://doi.org/10.1175/2009WAF2222286.1.

Demuth, J. L., M. DeMaria, and J. A. Knaff, 2006: Improvement of advanced microwave sounding unit tropical cyclone intensity and size estimation algorithms. *J. Appl. Meteor. Climatol.*, **45**, 1573–1581, https://doi.org/10.1175/JAM2429.1.

Dvorak, V. F., 1975: Tropical cyclone intensity analysis and forecasting from satellite imagery. *Mon. Wea. Rev.*, **103**, 420–430, https://doi.org/10.1175/1520-0493(1975)103<0420:TCIAAF>2.0.CO;2.

——, 1984: Tropical cyclone intensity analysis using satellite data. NOAA Tech. Rep. NESDIS 11, 47 pp., http://satepsanone.nesdis.noaa.gov/pub/Publications/Tropical/Dvorak_1984.pdf.

Emanuel, K. A., 1986: An air-sea interaction theory for tropical cyclones. Part I: Steady-state maintenance. *J. Atmos. Sci.*, **43**, 585–605, https://doi.org/10.1175/1520-0469(1986)043<0585:AASITF>2.0.CO;2.

——, 1987: The dependence of hurricane intensity on climate. *Nature*, **326**, 483–485, https://doi.org/10.1038/326483a0.

——, 2021: Response of global tropical cyclone activity to increasing CO_2: Results from downscaling CMIP6 models. *J. Climate*, **34**, 57–70, https://doi.org/10.1175/JCLI-D-20-0367.1.

GFS, 2021: Global forecast system. NOAA, accessed 1 March 2024, https://www.emc.ncep.noaa.gov/emc/pages/numerical_forecast_systems/gfs.php.

Gori, A., N. Lin, B. Schenkel, and D. Chavas, 2023: North Atlantic tropical cyclone size and storm surge reconstructions from 1950-present. *J. Geophys. Res. Atmos.*, **128**, e2022JD037312, https://doi.org/10.1029/2022JD037312.

Irish, J. L., and D. T. Resio, 2010: A hydrodynamics-based surge scale for hurricanes. *Ocean Eng.*, **37**, 69–81, https://doi.org/10.1016/j.oceaneng.2009.07.012.

Kanada, S., A. Wada, and M. Sugi, 2013: Future changes in structures of extremely intense tropical cyclones using a 2-km mesh nonhydrostatic model. *J. Climate*, **26**, 9986–10 005, https://doi.org/10.1175/JCLI-D-12-00477.1.

Kimberlain, T. B., E. S. Blake, and J. P. Cangialosi, 2016: Tropical cyclone report: Hurricane Patricia (EP202015), 20–24 October 2015. NHC Tech. Rep., 32 pp., https://www.nhc.noaa.gov/data/tcr/EP202015_Patricia.pdf.

Klotzbach, P. J., M. M. Bell, S. G. Bowen, E. J. Gibney, K. R. Knapp, and C. J. Schreck III, 2020: Surface pressure a more skillful predictor of normalized hurricane damage than maximum sustained wind. *Bull. Amer. Meteor. Soc.*, **101**, E830–E846, https://doi.org/10.1175/BAMS-D-19-0062.1.

——, D. R. Chavas, M. M. Bell, S. G. Bowen, E. J. Gibney, and C. J. Schreck III, 2022: Characterizing continental US hurricane risk: Which intensity metric is best? *J. Geophys. Res. Atmos.*, **127**, e2022JD037030, https://doi.org/10.1029/2022JD037030.

Knabb, R. D., D. P. Brown, and J. R. Rhome, 2006: Tropical cyclone report: Hurricane Rita, 18–26 September 2005. NHC Tech. Rep., 33 pp., https://www.nhc.noaa.gov/data/tcr/AL182005_Rita.pdf.

Knaff, J. A., and R. M. Zehr, 2007: Reexamination of tropical cyclone wind–pressure relationships. *Wea. Forecasting*, **22**, 71–88, https://doi.org/10.1175/WAF965.1.

——, and Coauthors, 2021: Estimating tropical cyclone surface winds: Current status, emerging technologies, historical evolution, and a look to the future. *Trop. Cyclone Res. Rev.*, **10**, 125–150, https://doi.org/10.1016/j.tcrr.2021.09.002.

Knutson, T. R., R. E. Tuleya, and Y. Kurihara, 1998: Simulated increase of hurricane intensities in a CO_2-warmed climate. *Science*, **279**, 1018–1021, https://doi.org/10.1126/science.279.5353.1018.

——, J. J. Sirutis, M. Zhao, R. E. Tuleya, M. Bender, G. A. Vecchi, G. Villarini, and D. Chavas, 2015: Global projections of intense tropical cyclone activity for the late twenty-first century from dynamical downscaling of CMIP5/RCP4.5 scenarios. *J. Climate*, **28**, 7203–7224, https://doi.org/10.1175/JCLI-D-15-0129.1.

——, and Coauthors, 2020: Tropical cyclones and climate change assessment: Part II: Projected response to anthropogenic warming. *Bull. Amer. Meteor. Soc.*, **101**, E303–E322, https://doi.org/10.1175/BAMS-D-18-0194.1.

Koba, H., T. Hagiwara, S. Osano, and S. Akashi, 1990: Relationship between the CI-number and central pressure and maximum wind speed in typhoons. *J. Meteor. Res.*, **42**, 59–67.

Kossin, J. P., K. A. Emanuel, and G. A. Vecchi, 2014: The poleward migration of the location of tropical cyclone maximum intensity. *Nature*, **509**, 349–352, https://doi.org/10.1038/nature13278.

Lin, N., and D. Chavas, 2012: On hurricane parametric wind and applications in storm surge modeling. *J. Geophys. Res.*, **117**, D09120, https://doi.org/10.1029/2011JD017126.

Lu, K.-Y., and D. R. Chavas, 2022: Tropical cyclone size is strongly limited by the Rhines scale: Experiments with a barotropic model. *J. Atmos. Sci.*, **79**, 2109–2124, https://doi.org/10.1175/JAS-D-21-0224.1 .

Saha, S., and Coauthors, 2014: The NCEP Climate Forecast System version 2. *J. Climate*, **27**, 2185–2208, https://doi.org/10.1175/JCLI-D-12-00823.1.

Sampson, C. R., and A. J. Schrader, 2000: The Automated Tropical Cyclone Forecasting System (version 3.2). *Bull. Amer. Meteor. Soc.*, **81**, 1231–1240, https://doi.org/10.1175/1520-0477(2000)081<1231:TATCFS>2.3.CO;2.

——, E. M. Fukada, J. A. Knaff, B. R. Strahl, M. J. Brennan, and T. Marchok, 2017: Tropical cyclone gale wind radii estimates for the western North Pacific. *Wea. Forecasting*, **32**, 1029–1040, https://doi.org/10.1175/WAF-D-16-0196.1.

Schenkel, B. A., D. Chavas, N. Lin, T. Knutson, G. Vecchi, and A. Brammer, 2023: North Atlantic tropical cyclone outer size and structure remain unchanged by the late twenty-first century. *J. Climate*, **36**, 359–382, https://doi.org/10.1175/JCLI-D-22-0066.1.

Schott, T., and Coauthors, 2012: The Saffir-Simpson hurricane wind scale. National Weather Services, National Hurricane Center, National Oceanic and Atmospheric Administration (NOAA) factsheet, 4 pp., https://mail.hwn.org/media/pdf/sshws.pdf.

Schwerdt, R. W., F. P. Ho, and R. R. Watkins, 1979: Meteorological criteria for standard project hurricane and probable maximum hurricane windfields, Gulf and east coasts of the United States. NOAA Tech. Rep. NWS 23, 317 pp., https://www.weather.gov/media/owp/oh/hdsc/docs/TR23.pdf.

Stansfield, A. M., and K. A. Reed, 2021: Tropical cyclone precipitation response to surface warming in aquaplanet simulations with uniform thermal forcing. *J. Geophys. Res. Atmos.*, **126**, e2021JD035197, https://doi.org/10.1029/2021JD035197.

Torn, R. D., and C. Snyder, 2012: Uncertainty of tropical cyclone best-track information. *Wea. Forecasting*, **27**, 715–729, https://doi.org/10.1175/WAF-D-11-00085.1.

Tran, T. L., E. A. Ritchie, S. E. Perkins-Kirkpatrick, H. Bui, and T. M. Luong, 2022: Future changes in tropical cyclone exposure and impacts in Southeast Asia from CMIP6 pseudo-global warming simulations. *Earth's Future*, **10**, e2022EF003118, https://doi.org/10.1029/2022EF003118.

Uhlhorn, E. W., and D. S. Nolan, 2012: Observational undersampling in tropical cyclones and implications for estimated intensity. *Mon. Wea. Rev.*, **140**, 825–840, https://doi.org/10.1175/MWR-D-11-00073.1.

Zarzycki, C. M., P. A. Ullrich, and K. A. Reed, 2021: Metrics for evaluating tropical cyclones in climate data. *J. Appl. Meteor. Climatol.*, **60**, 643–660, https://doi.org/10.1175/JAMC-D-20-0149.1.

Zhai, A. R., and J. H. Jiang, 2014: Dependence of US hurricane economic loss on maximum wind speed and storm size. *Environ. Res. Lett.*, **9**, 064019, https://doi.org/10.1088/1748-9326/9/6/064019.